Combined State and Parameter Estimation of Lithium-Ion Battery With Active Current Injection

Ziyou Song, *Member, IEEE*, Hao Wang, Jun Hou, *Member, IEEE*, Heath F. Hofmann, *Senior Member, IEEE*, and Jing Sun, *Fellow, IEEE*

***Abstract*—Estimating the State-of-Charge (SoC) and State-of-Health (SoH), together with the parameters used in representing the dynamics of a lithium-ion battery, is essential to ensure optimal and reliable operation. However, this simultaneous estimation can take a significant amount of time to converge, and the estimation accuracy is limited by measurement noise and model inaccuracy. Note that for overactuated systems (e.g., hybrid energy storage systems and hybrid electric vehicles), the overactuation feature can be exploited to optimize the battery current profile for the estimation purpose. This article shows the potential to improve estimation accuracy when the desired current is actively injected and the estimation algorithm is properly structured. Specifically, by incorporating a high-pass filter, battery parameters can be independently characterized by injecting high-frequency and medium-frequency currents, and battery SoC/SoH can then be estimated sequentially from the estimated parameters. A Cramer–Rao bound analysis shows that the accuracy of the proposed sequential estimation is much better than the case where all parameters and states are simultaneously estimated. The analysis is verified by simulation and experimental results. We point out that for battery-only applications (e.g., electric vehicles); the proposed method has limitations, as generally, the battery current profile cannot be changed.**

***Index Terms*—Cramer-rao bounds, estimation error, lithium batteries, parameter estimation, sequential analysis, state estimation.**

I. Introduction

LITHIUM-ION batteries have been widely used in many applications, such as electric vehicles and renewable energy systems [1]. Online monitoring of State-of-Charge (SoC) and State-of-Health (SoH) plays an important role in ensuring safe, reliable, and efficient operation [2]. However, when simultaneously estimating all parameters and states of the battery, the estimation can take a significant amount of time to converge, and its accuracy can be compromised when considering model uncertainty and measurement noise [3].

Manuscript received February 16, 2019; revised May 10, 2019 and July 22, 2019; accepted October 1, 2019. Date of publication October 3, 2020; date of current version January 10, 2020. This work was supported by the U.S. Office of Naval Research under Grants N00014-16-1-3108 and N00014-18-2330. Recommended for publication by Associate Editor S. Williamson. *(Corresponding author: Ziyou Song.)*

Z. Song, H. Wang, and J. Sun are with the Department of Naval Architecture and Marine Engineering, University of Michigan, Ann Arbor, MI 48109 USA (e-mail: ziyou.songthu@gmail.com; auautowang@umich.edu; jingsun@umich.edu).

J. Hou and H. F. Hofmann are with the Department of Electrical Engineering and Computer Science, University of Michigan, Ann Arbor, MI 48109 USA (e-mail: junhou@umich.edu; hofmann@umich.edu).

Color versions of one or more of the figures in this article are available online at http://ieeexplore.ieee.org.

Digital Object Identifier 10.1109/TPEL.2019.2945513

Most of the literature on battery state and parameter estimation has focused on battery models [4] and estimation algorithms [5]. While these studies are important, the input–output data used play a significant role in the estimation performance [6]. A persistently exciting (PE) input condition must be necessarily satisfied to ensure that all parameters can converge to the actual values [7]. In addition, most existing estimation approaches use the data indiscriminately without exploiting the sensitivity of the data to the specific parameters to be identified [8]. The estimation accuracy will be impaired when data without a sufficient "richness" are used [9], [10].

In recent years, more attention has been paid to the impact of data on estimation performance. Analytical results provided in [11] and [12] use the Fisher information matrix and Cramer–Rao (CR) bounds to analyze the influence of data on estimation accuracy. Rothenberger *et al*. optimized the battery current profile to maximize the Fisher information matrix for a better estimation performance [13], [14]. Lin and Stefanopoulou derived analytic bounds on the estimation accuracy of SoC, capacity, and ohmic resistance under various circumstances [6]. The connection between the excitation and the SoC estimation error considering measurement noise/bias [15], model uncertainties [16], and estimation algorithms has also been addressed.

However, in the case where all battery parameters and states are estimated simultaneously, the estimation performance is limited even when the battery current profile is well-designed [17]. This is caused by the fact that the state and parameter estimation problems are inherently intertwined, and noise is introduced in the measurement. The separation of state and parameter estimation, which could lead to reduced uncertainty in each estimation problem, however, has not been explored. Based on analysis of the first-order equivalent circuit model (ECM), it has been shown that it is possible to estimate battery parameters/states sequentially by incorporating a high-pass filter and actively injecting current signals to improve the estimation accuracy. Performance of the sequential algorithm has also been demonstrated [18]. Such a sequential algorithm is, therefore, adopted in this article. We note that the sequential algorithm was designed for overactuated systems (e.g., hybrid electric vehicles and the battery/supercapacitor hybrid energy storage system), since the overactuation feature can be exploited for the active current injection.

This article focuses on establishing the properties of the sequential algorithm and the optimization of the inputs for estimation. The main contributions of this article include the

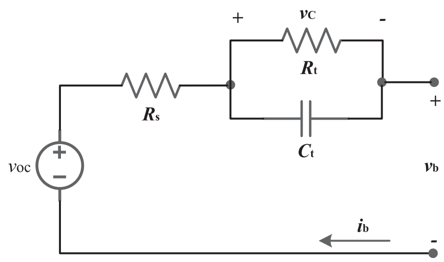

Fig. 1. First-order ECM for battery.

following aspects. First, the time-averaged CR bound, which indicates the lower bound of the estimation error covariance of unbiased estimation, is used to establish the advantage of the sequential algorithm when compared to the multiparameter case where all parameters and states are estimated concurrently. Second, the influence of frequency on the estimation performance is investigated for the sequential algorithm to optimize the current profile. Third, simulations are conducted considering noise, and the effectiveness of the sequential algorithm is validated. Finally, initial experimental results are provided to further verify the proposed algorithm.

The rest of this article is organized as follows. In Section II, the first-order ECM battery model is described and the dynamics are analyzed. In Section III, the time-averaged CR bound is briefly introduced and the CR bound analysis is performed. Simulation results are shown in Section IV. Experimental results are presented in Section V. Section VI concludes this article.

II. System Description

The state estimation of lithium-ion batteries, including battery SoC and SoH, is an important task in practical applications. To perform this task, model-based algorithms have been widely studied. Generally, the model parameters are significantly influenced by battery degradation and operating conditions, therefore, the model parameters should be estimated together with the battery states. However, it is challenging to simultaneously estimate all parameters and states given model inaccuracy, uncertainties, and measurement noise. In this section, the battery dynamics are analyzed, and the possibility of separating different dynamic components in the frequency domain is investigated to decompose the coupled estimation problem.

There are various models for lithium-ion batteries, such as the ECM [4], impedance model [19], and electrochemical model [20]. While the more complex models (e.g., the electrochemical model) are more accurate, the first-order ECM is widely used in practical applications given its simplicity and sufficient accuracy [4]. We point out that even though the analysis in this article focuses on the first-order ECM, the proposed methodology can be generalized to other models. As shown in Fig. 1, the battery terminal voltage and current are denoted as $v_{\rm b}$ and $i_{\rm b}$, respectively. The ECM dynamics can be presented as follows:

$$\begin{cases} \dot{v}_{\rm C} = -\frac{1}{C_{\rm t} R_{\rm t}} v_C + \frac{1}{C_{\rm t}} i_{\rm b} \\ v_{\rm b} = v_{\rm OC} - R_{\rm s} i_{\rm b} - v_{\rm C} \end{cases} \tag{1}$$

TABLE I
Specification for the 18650 Battery Cell

Parameter	Value
Nominal Voltage (V)	3.63
Cell Capacity (Ah)	2.44
Ohmic Resistance $R_{\rm s}$ (mΩ)	~100
Diffusion Resistance $R_{\rm t}$ (mΩ)	~30
Time Constant τ (s)	~15
Discharge/Charge Efficiency η (%)	98
OCV-SoC Slope a (mV/100%)	~8.845
Voltage Measurement Noise $\sigma_{\rm V}$ (mV)	20

where $v_{\rm C}$ is the voltage of *RC* pair. The open circuit voltage (OCV)–SoC relationship is given as [21]

$$v_{\rm OC}(z) = K_0 - \frac{K_1}{z} - K_2 z + K_3 \ln(z) + K_4 \ln(1-z) \tag{2}$$

where $K_{0\text{-}4}$ are the model coefficients and z is the normalized SoC. The SoC dynamic is described as [22]

$$z = z_0 - \int_{t_0}^{t} \frac{\eta}{Q_{\rm b}} i_{\rm b}(t) dt \tag{3}$$

where z_0 is the initial SoC, η is the charging/discharging efficiency, t_0 is the start time, and $Q_{\rm b}$ is the battery capacity. The slope of the OCV–SoC curve is constant for most battery chemistries within the normal operating range [23], [24]. Consequently, (2) is linearized to simplify the CR bound analysis in the following section:

$$v_{\rm OC}(t) = a \left(z_0 - \int_{t_0}^{t} \frac{\eta i_{\rm b}(\upsilon)}{Q_{\rm b}} {\rm d}\upsilon \right) + b \tag{4}$$

where a and b are the coefficients of the linearized OCV–SoC function. The battery SoC and SoH are represented by z_0 and $Q_{\rm b}$, respectively. An 18650 lithium-ion battery cell made by Samsung is considered, and its parameters are listed in Table I. The coefficients $K_{0\text{–}4}$ of the OCV–SoC for the adopted cell are $2.6031, 0.0674, -1.527, 0.6265$, and -0.0297, respectively. The battery parameters and OCV–SoC coefficients were obtained by conducting hybrid pulse power capability (HPPC) and static capacity tests on the adopted battery cell.

For the combined state and parameter estimation problem studied in this article, the following assumptions can be made:

1) the initial value of $v_{\rm C}$ is 0;
2) the values of $R_{\rm s}$, $R_{\rm t}$, and τ are constant in the estimation process, since they vary much more slowly than the battery SoC [25].

Based on (1)–(3), the transfer function from $i_{\rm b}$ to $v_{\rm b}$ can be given as

$$v_{\rm b}(s) = \left[\frac{a z_0}{s} + \frac{b}{s}\right] - \left[\frac{a}{s}\frac{\eta}{Q_{\rm b}} i_{\rm b}(s)\right] - \left[R_{\rm s} i_{\rm b}(s)\right] - \left[\frac{R_{\rm t}}{1+\tau s} i_{\rm b}(s)\right] \tag{5}$$

where s is the complex Laplace variable. Note that the battery terminal voltage expression includes four components, with each term associated with a specific subset of parameters. The first term is due to the initial SoC. The second is related to the SoC variation, and is significantly influenced by the battery capacity Q_{b}. The third and fourth components are related to the ohmic resistance and the *RC* pair, respectively.

These four components of the battery voltage have significantly different characteristics in the frequency domain; a property will be exploited in this article by incorporating filters and actively injecting current signals that decompose the state and parameter estimation problem.

Consider passing the battery voltage and current measurements through a first-order high-pass filter

$$v_{\mathrm{bf}}(s) = \frac{T_{\mathrm{c}} s}{1+T_{\mathrm{c}} s} v_{\mathrm{b}}(s), \quad i_{\mathrm{bf}}(s) = \frac{T_{\mathrm{c}} s}{1+T_{\mathrm{c}} s} i_{\mathrm{b}}(s)$$

where T_{c} is the time coefficient of the high-pass filter, and v_{bf} and i_{bf} are the filtered battery voltage and current, respectively. The filtered system can be described as

$$v_{\mathrm{bf}}(s) = v_{\mathrm{c1}}(s) - v_{\mathrm{c2}}(s) - v_{\mathrm{c3}}(s) - v_{\mathrm{c4}}(s) \tag{6}$$

where

$$v_{\mathrm{c1}}(s) = \frac{(az_0+b)\,T_{\mathrm{c}}}{1+T_{\mathrm{c}} s}, \quad v_{\mathrm{c2}}(s) = \frac{a}{s}\frac{\eta}{Q_{\mathrm{b}}} i_{\mathrm{bf}}(s)$$

$$v_{\mathrm{c3}}(s) = R_{\mathrm{s}} i_{\mathrm{bf}}(s), \quad v_{\mathrm{c4}}(s) = \frac{R_{\mathrm{t}}}{1+\tau s} i_{\mathrm{bf}}(s)$$

and v_{c1}, v_{c2}, v_{c3}, and v_{c4} are the terms associated with filtered initial SoC, SoC variation, ohmic resistance, and *RC* pair voltage components, respectively. After filtering, the response to the initial SoC is given as

$$v_{\mathrm{c1}}(t) = \mathcal{L}^{-1}\left\{\frac{(az_0+b)\,T_{\mathrm{c}}}{1+T_{\mathrm{c}} s}\right\} = (az_0+b)\,e^{-\frac{t}{T_{\mathrm{c}}}} \to 0 \tag{7}$$

which will vanish over time and can, therefore, be neglected. A sinusoidal battery current, which is frequently used for parameter estimation, is considered to analyze the battery dynamics

$$\begin{cases} i_{\mathrm{b}}(t) = M\ \cos(\omega t) \\ i_{\mathrm{b}}(s) = \frac{Ms}{s^2+\omega^2} \end{cases} \tag{8}$$

where M is the current magnitude and ω is the current frequency. The filtered voltage components v_{c2}, v_{c3}, and v_{c4} asymptotically converge to

$$\begin{cases} v_{\mathrm{c2}}(t) \to -Ma\eta T_{\mathrm{c}} \frac{T_{\mathrm{c}}\omega\ \sin(\omega t) - \cos(\omega t)}{Q_{\mathrm{b}}(1+T_{\mathrm{c}}^2\omega^2)} \\ v_{\mathrm{c3}}(t) \to -MR_{\mathrm{s}} T_{\mathrm{c}}\omega \frac{T_{\mathrm{c}}\omega\ \cos(\omega t) - \sin(\omega t)}{1+T_{\mathrm{c}}^2\omega^2} \\ v_{\mathrm{c4}}(t) \to -MR_{\mathrm{t}} T_{\mathrm{c}}\omega \frac{\left[(T_{\mathrm{c}}\omega+\omega\tau)\cos(\omega t) + \left(T_{\mathrm{c}}\omega^2\tau - 1\right)\sin(\omega t)\right]}{(1+T_{\mathrm{c}}^2\omega^2)(1+\tau^2\omega^2)}. \end{cases} \tag{9}$$

As shown in (9), v_{c2}, v_{c3}, and v_{c4} converge to sinusoidal waveforms. To investigate the influence of frequency ω on the battery dynamics, the amplitudes of v_{c2}, v_{c3}, and v_{c4} at different frequencies are shown in Fig. 2 for $T_{\mathrm{c}} = 80$ s. As shown in Fig. 2, when the current frequency is "high" (i.e., >0.1 Hz), the battery voltage is dominated by the term that is associated with the ohmic resistance. When the current frequency is "medium" (e.g., 0.004 Hz), the SoC variation voltage can be neglected.

The reason is that only the low-frequency current induces a significant SoC change. When the current frequency is "low" (e.g., 0.0004 Hz), v_{c2}, v_{c3}, and v_{c4} should all be considered. Therefore, by incorporating a high-pass filter, the battery voltage components can be "stripped out" by injecting battery current waveforms of different frequencies. We point out that the analysis shown earlier should be conducted for different battery chemistries, where the frequency ranges may slightly change.

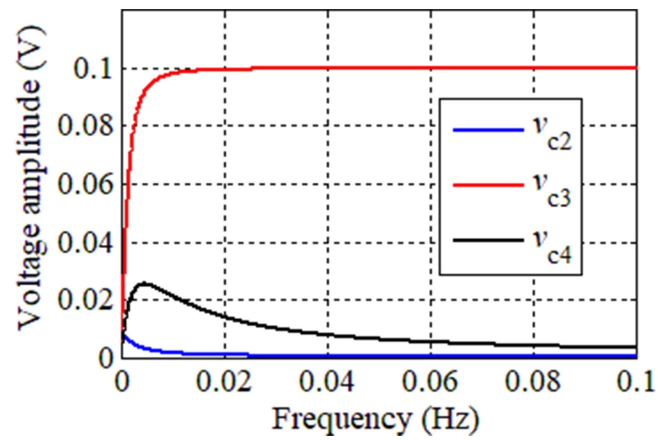

Fig. 2. Battery voltage components at various current frequencies.

III. CR Bound Analysis

A. Time-Averaged CR Bound

The CR bound can be used to quantify estimation accuracy [13]. The process for computing the time-averaged CR bound is briefly introduced as follows. The sensitivity of the voltage measurement v_{b} to the ith parameter θ_i in the time domain can be expressed using the inverse Laplace transform $\mathcal{L}^{-1}$

$$\frac{\partial v_{\mathrm{b}}}{\partial \theta_i}(t) = \mathcal{L}^{-1}\left[\frac{\partial v_{\mathrm{b}}}{\partial \theta_i}(s)\right]. \tag{10}$$

Assuming Gaussian noise in the measurement of v_{b}, the time-averaged Fisher information matrix $\bar{\mathbf{F}}_{\mathrm{c}}$ can be calculated when the battery current $i_{\mathrm{b}}(t)$ is a periodic signal with period $2\pi/\omega$. The details of this calculation are provided in as follows:

$$\bar{\mathbf{F}}_{\mathrm{c}} = \frac{1}{\sigma_{\mathrm{V}}^2}\frac{\omega}{2\pi}$$
$$\begin{pmatrix} \int_0^{\frac{2\pi}{\omega}} \left(\frac{\partial v_{\mathrm{b}}}{\partial \theta_1}\right)^2 \mathrm{d}t & \int_0^{\frac{2\pi}{\omega}} \left(\frac{\partial v_{\mathrm{b}}}{\partial \theta_1}\frac{\partial v_{\mathrm{b}}}{\partial \theta_2}\right)\mathrm{d}t & \cdots & \int_0^{\frac{2\pi}{\omega}} \left(\frac{\partial v_{\mathrm{b}}}{\partial \theta_1}\frac{\partial v_{\mathrm{b}}}{\partial \theta_N}\right)^2 \mathrm{d}t \\ \int_0^{\frac{2\pi}{\omega}} \left(\frac{\partial v_{\mathrm{b}}}{\partial \theta_2}\frac{\partial v_{\mathrm{b}}}{\partial \theta_1}\right)\mathrm{d}t & \int_0^{\frac{2\pi}{\omega}} \left(\frac{\partial v_{\mathrm{b}}}{\partial \theta_2}\right)^2 \mathrm{d}t & \cdots & \int_0^{\frac{2\pi}{\omega}} \left(\frac{\partial v_{\mathrm{b}}}{\partial \theta_2}\frac{\partial v_{\mathrm{b}}}{\partial \theta_N}\right)\mathrm{d}t \\ \vdots & \vdots & \vdots & \\ \int_0^{\frac{2\pi}{\omega}} \left(\frac{\partial v_{\mathrm{b}}}{\partial \theta_N}\frac{\partial v_{\mathrm{b}}}{\partial \theta_1}\right)\mathrm{d}t & \int_0^{\frac{2\pi}{\omega}} \left(\frac{\partial v_{\mathrm{b}}}{\partial \theta_N}\frac{\partial v_{\mathrm{b}}}{\partial \theta_2}\right)\mathrm{d}t & \cdots & \int_0^{\frac{2\pi}{\omega}} \left(\frac{\partial v_{\mathrm{b}}}{\partial \theta_N}\right)^2 \mathrm{d}t \end{pmatrix} \tag{11}$$

where $\boldsymbol{\theta} = [\theta_1, \theta_2, \ldots, \theta_N]$ is the vector of parameters to be identified and σ_{V}^2 is the variance of the battery voltage measurement noise. The CR bounds can then be obtained by inverting the Fisher information matrix

$$\mathrm{cov}(\theta_i) \geq \underline{\sigma}^2(\theta_i) = \mathrm{diag}\left(\overline{\mathbf{F}}_{\mathrm{c}}^{-1}\right)_i \tag{12}$$

where the over bar symbol (–) denotes a time-averaged value, $\mathrm{cov}(\theta_i)$ is the variance of the estimation error for θ_i, $\underline{\sigma}^2(\theta_i)$ is the CR lower bound of θ_i, indicating the minimum achievable variance, and $\mathrm{diag}(\overline{\mathbf{F}}_{\mathrm{c}}^{-1})_i$ is the ith diagonal element of $\overline{\mathbf{F}}_{\mathrm{c}}^{-1}$.

B. Sequential Algorithm

The sequential algorithm includes three steps, which are as follows.

Step #1: The ohmic resistance is estimated by using a high-pass filter and injecting a high-frequency current.

Step #2: The estimated ohmic resistance is then used in the estimation of R_{t} and τ, which are estimated by using a high-pass filter and injecting medium-frequency current.

Step #3: Based on the estimated R_{s}, R_{t}, and τ, the SoC and SoH are then simultaneously estimated.

The CR bounds of the filtered system are derived following the process shown in Section III-A. Based on (6), it can be seen that by injecting high-frequency current, the filtered system can be simplified as

$$v_{\mathrm{bf}}(s) \approx -R_{\mathrm{s}} i_{\mathrm{bf}}(s). \tag{13}$$

Therefore, the ohmic resistance R_{s} can be estimated solely in the first step. By using the sinusoidal current shown in (8), the asymptotic sensitivity and the time-averaged CR bound of R_{s} can be given as

$$\frac{\partial v_{\mathrm{bf}}}{\partial R_{\mathrm{s}}}(t) = -MT_{\mathrm{c}}\omega \frac{T_{\mathrm{c}}\omega\cos(\omega t) - \sin(\omega t)}{T_{\mathrm{c}}^2\omega^2 + 1}$$
$$\underline{\sigma}(R_{\mathrm{s}}) = \frac{\sqrt{2}\sigma_{\mathrm{V}}\sqrt{T_{\mathrm{c}}^2\omega^2+1}}{MT_{\mathrm{c}}\omega}. \tag{14}$$

This shows that the estimation accuracy of R_{s} can be improved by decreasing the voltage measurement noise σ_{V} and the cutoff frequency (i.e., $1/T_{\mathrm{c}}$) as well as increasing the current amplitude and frequency. Note that $1/T_{\mathrm{c}}$ cannot be too low, especially when the battery current involves medium-frequency components, as the dynamics of the *RC* pair should also be considered and it makes the simplification in (13) inaccurate, as shown in Fig. 2. When the medium-frequency current is injected, the filtered system can be simplified as follows:

$$V_{\mathrm{bf}}(s) = -\hat{R}_{\mathrm{s}} i_{\mathrm{bf}}(s) - \frac{R_{\mathrm{t}}}{1+\tau s} i_{\mathrm{bf}}(s) \tag{15}$$

where $\hat{R}_{\mathrm{s}}$ is the estimated ohmic resistance that can be used in the second step to estimate R_{t} and τ. The asymptotic sensitivities and time-averaged CR bounds of R_{t} and τ can, therefore, be obtained as follows:

$$\frac{\partial v_{\mathrm{bf}}}{\partial R_{\mathrm{t}}}(t) = -MT_{\mathrm{c}}\omega \frac{T_{\mathrm{c}}\omega\cos(\omega t) - \sin(\omega t) + \omega\tau\cos(\omega t)}{(T_{\mathrm{c}}^2\omega^2+1)(\tau^2\omega^2+1)}$$
$$\frac{\partial v_{\mathrm{bf}}}{\partial \tau}(t) = \frac{\left[\left(T_{\mathrm{c}}\omega - T_{\mathrm{c}}\omega^3\tau^2 + 2\omega\tau\right)\sin(\omega t) + \left(1-\omega^2\tau^2 - 2T_{\mathrm{c}}\omega^2\tau\right)\cos(\omega t)\right]}{(T_{\mathrm{c}}^2\omega^2+1)(\tau^2\omega^2+1)^2/(-MT_{\mathrm{c}}\omega^2 R_{\mathrm{t}})}$$
$$\underline{\sigma}(R_{\mathrm{t}}) = \frac{\sigma_{\mathrm{V}}\left(\tau^2\omega^2+1\right)\sqrt{2(T_{\mathrm{c}}^2\omega^2+1)}}{MT_{\mathrm{c}}\omega}$$
$$\underline{\sigma}(\tau) = \frac{\sigma_{\mathrm{V}}\left(\tau^2\omega^2+1\right)\left(T_{\mathrm{c}}^2\omega^2+1\right)\sqrt{2(T_{\mathrm{c}}^2\omega^2+1)}}{MT_{\mathrm{c}}\omega^2 R_{\mathrm{t}}}. \tag{16}$$

It is clear that the estimation of the *RC* pair (i.e., R_{t} and τ) can be improved by decreasing σ_{V} (i.e., measurement noise) and increasing M (i.e., signal amplitude). However, the influences of $1/T_{\mathrm{c}}$ and ω are complex and will be numerically analyzed. Based on the abovementioned estimated parameters, the battery SoC and SoH can be estimated using (5). The asymptotic sensitivities and time-averaged CR bounds of z_0 and $1/Q_{\mathrm{b}}$ are

$$\frac{\partial v_{\mathrm{bf}}}{\partial z_0}(t) = a, \quad \frac{\partial v_{\mathrm{bf}}}{\partial(1/Q_{\mathrm{b}})}(t) = \frac{Ma\eta\,\sin(\omega t)}{\omega}$$
$$\underline{\sigma}(z_0) = \frac{\sigma_{\mathrm{V}}}{a}, \quad \underline{\sigma}(1/Q_{\mathrm{b}}) = \frac{\sqrt{2}\sigma_{\mathrm{V}}\omega}{Ma\eta}. \tag{17}$$

The estimation of SoC only depends on the OCV slope a. The estimation accuracy of $1/Q_{\mathrm{b}}$ can be improved by decreasing the current frequency as the battery capacity influences the battery terminal voltage via the SoC change, and therefore, the detectable voltage variation requires a large SoC change. It is obvious and intuitive that the estimation accuracy can be increased by reducing noise and increasing current amplitude, as the SoC estimation accuracy can be improved when the battery has a more detectable voltage change. We point out that the quantified relationships presented in this article can be used to evaluate the influences of different estimation techniques, which involve different amounts of uncertainty, on the estimation accuracy. Specifically, the improvement of the sequential algorithm is quantified when compared to the case where all parameters/states are estimated simultaneously, as will be shown in the sequel. The quantified relationships are important in the design of different estimation techniques and theoretically prove the effectiveness of the new design.

In this article the CR bounds of estimated parameters/states under the sequential algorithm are compared with the multiparameter case. According to the analysis in [17], two sinusoidal waveforms with the same amplitudes and with frequencies of ω and 5ω are used in the multiparameter case to persistently excite the battery. The same amplitudes are chosen to simplify the analysis, whereas the frequencies of ω and 5ω were determined based on the CR bound analysis, which shows that the good performance is achieved when the frequency ratio is 5 [17].

Regarding the sequential algorithm, high-pass filters are adopted to ensure that the battery dynamics induced by the injected signals can be extracted for estimation purposes. The cutoff frequencies of the high-pass filters for estimating ohmic resistance and *RC* pair were set to 0.05 and 0.001 Hz, respectively, as the frequencies of the injected current were 0.5 and 0.02 Hz. In the comparison, the single-parameter case, which only estimates one parameter (or state) and assumes all other parameters/states to be well known, is considered as the benchmark. The CR bounds of SoC are not shown because they are same for all cases. The CR bounds are shown in Fig. 3, and some remarks can be given as follows.

Remark 1: The single-parameter case has the best estimation performance over all conditions since the least uncertainty is involved.

Remark 2: For R_{s}, the estimation performance of the sequential algorithm is slightly worse than the multiparameter case

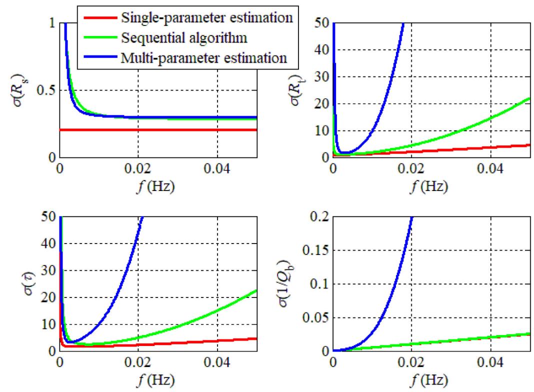

Fig. 3. CR bounds results.

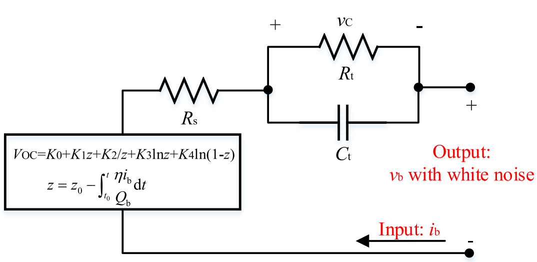

Fig. 4. Simulation model of the first-order circuit.

at low frequency due to the use of high-pass filter. However, when the frequency increases, the estimation performance of the sequential algorithm is better due to the reduction of uncertainty. In addition, the sequential algorithm achieves much better performance when estimating the *RC* pair.

Remark 3: The SoC estimation accuracy of the sequential algorithm is the same as that of the single-parameter case, and much better than the multiparameter case.

Remark 4: For the multiparameter case, there is a tradeoff between R_s and *RC* pair. As a result, the optimal frequencies, which can achieve a good performance for all estimated parameters, are set to 0.002 and 0.01 Hz.

IV. Simulation Results

To verify the analysis in Section III, simulations were conducted based on the first-order ECM, as shown in Fig. 4. The battery parameters listed in Table I were adopted. Note that the OCV–SoC curve of lithium-ion batteries generally presents nonlinear characteristics. The OCV–SoC curve for the studied battery cell is shown in Fig. 5, which indicates that the OCV–SoC curve can be approximately linearized over the SoC range of 50%–90% where the slope is approximately 8.8 mV per 1% SoC variation. It means that when the battery SoC changes 1%, the battery OCV changes 8.8 mV averagely over the SoC range of 50%–90%. To simplify the CR bound analysis, a linearized OCV–SoC curve is used, whereas the nonlinear OCV–SoC curve is used in the simulation model as well as in the sequential algorithm. In addition, in the simulation, white noise signals are generated in MATLAB and then added to the voltage measurement generated by the simulation model shown in Fig. 4.

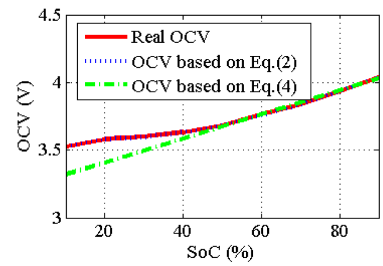

Fig. 5. OCV–SoC curve of the adopted Samsung ICR18650-26H cell.

In the multiparameter case, the multiscale extended Kalman filter (EKF), which has been proven to have good performance [3], is used to simultaneously estimate all parameters and states. The optimal current profile, which includes three sinusoidal waveforms with frequencies of 0.002, 0.01, and 0.005 Hz, is used in the multiparameter case. We point out that two frequencies are included in the CR bound analysis for the four estimated parameters, since the SoC estimation is independent of the current frequency. However, SoC is also estimated in the simulation, therefore, the 0.005 Hz waveform is an additional component to persistently excite the system because in total, five parameters/states are estimated [7]. For the sequential algorithm, according to the CR bound results shown in Fig. 3, we incorporate a first-order high-pass filter (3-dB bandwidth of 0.05 Hz) and inject a 0.5-Hz sinusoidal current with an amplitude of 0.5 C (i.e., 1.22 A) to estimate R_s. This value is then used in the second step to estimate R_t and τ by injecting a 0.02-Hz sinusoidal current with an amplitude of 0.5 C. A first-order high-pass filter with 3-dB bandwidth at 0.001 Hz is adopted. The EKF is used in the abovementioned steps. After obtaining the abovementioned parameters, a combined SoC/SoH estimation is finally conducted using the dual EKF. Two sinusoidal currents (0.01 and 0.05 Hz) and a dc current (all current amplitudes are 0.02 C rate) are used. For a fair comparison, the initial guesses of the estimated parameters/states are the same for both the multiparameter and sequential algorithm cases, which are set to $[R_s(0)\ R_t(0)\ \tau(0)\ 1/Q_b(0)\ \mathrm{SoC}(0)]^T = [0.02\ 0.01\ 10\ 1/2\ 1]^T$. White noise with the standard variance of 10 mV is added to the battery voltage measurement. Note that the frequency of the injected current depends on the battery parameters. For example, for some battery types, the time constant of the *RC* pair is much smaller than the one of the studied battery cell. As a result, the frequencies of the injected current for ohmic resistance and *RC* pair estimation should be increased to strip out the battery dynamics dominated by the parameter in question. The frequency can be selected based on the battery dynamic analysis, as shown in Fig. 2. We point out that the selected frequencies for the injected current may not be able to be adopted to other types of batteries. But the same analysis presented in this article can be followed for the frequency selection, which does not influence the effectiveness of the proposed algorithm.

The simulation results are shown in Figs. 6 and 7. Note that the actual states are generated using the simulation model shown in Fig. 4 together with the battery parameters given in Table I.

Regarding R_s, both cases have satisfactory estimation performance. In addition, although the best performance of the

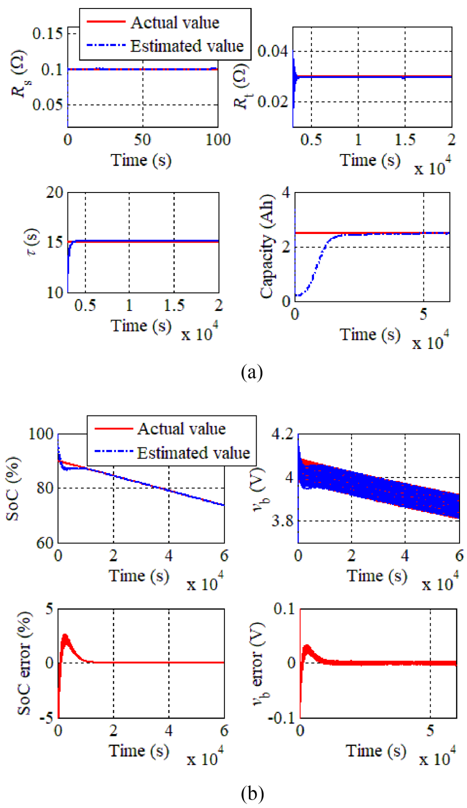

Fig. 6. Simulation results of the sequential algorithm. (a) Parameter estimation results. (b) State estimation results.

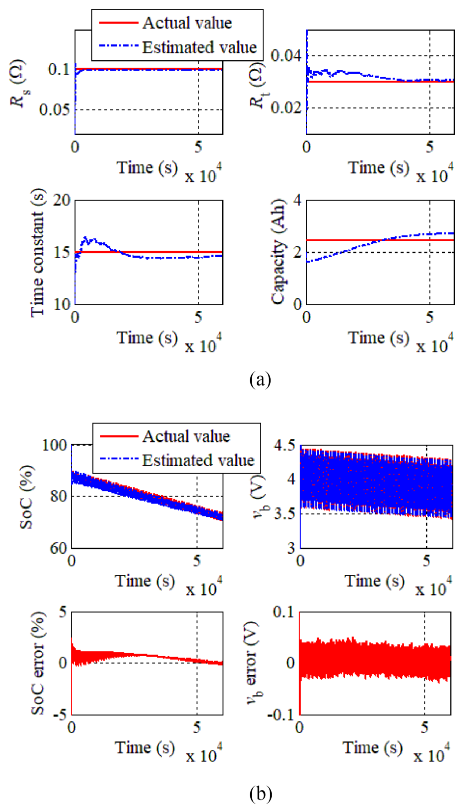

Fig. 7. Simulation results of the multiparameter case. (a) Parameter estimation results. (b) State estimation results.

multiparameter case is obtained using the optimal current profile, the sequential algorithm still achieves much better performance when estimating *RC* pair parameters, SoC, and SoH. The CR bound analysis shown in Section III is, therefore, verified. When the estimation of parameters and states can be separated and conducted sequentially, the estimation accuracy can be significantly improved since less uncertainty is involved.

V. Experimental Results

To verify the CR bound analysis and the effectiveness of the sequential algorithm, experiments were conducted using a lithium-ion battery cell, whose parameters can be found in Table I. As shown in Fig. 8, the test bench consists of an ARBIN BT2000 tester, a temperature chamber, and the *MITS pro* system used for programming the current profile and monitoring the battery [26]. The battery cell is placed in the temperature chamber, which is accurately controlled to provide a constant temperature environment during the experiment. The voltage and current of the battery cell are measured by the ARBIN tester and then sent to a computer through TCP/IP communication. Unlike the simulation, the battery parameters are changing in the experiment as they depend on SoC, and errors caused by unmodeled dynamics are also introduced. The "actual values" of battery parameters were calculated based on the HPPC test. The experiment was conducted at 20 °C and an initial battery SoC of 60%. The initial values of the estimated parameters are chosen to be $[\hat{R}_s(0)\ \widehat{R_t(0)}\ \hat{\tau}(0)\ \hat{Q}_b(0)] = [0.02\ 0.03\ 15\ 2]$, and the initial values of estimated SoC and v_C were set to 30% and 0 V, respectively.

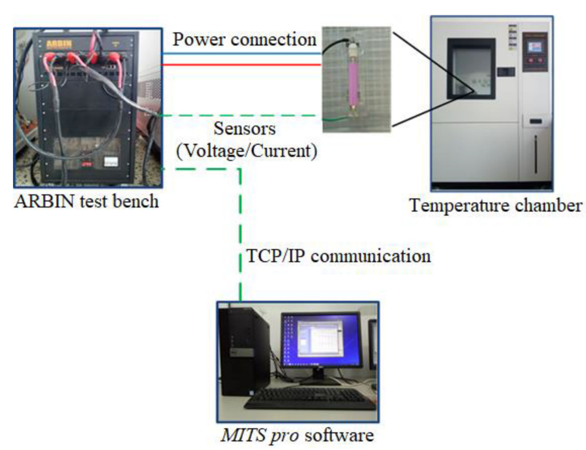

Fig. 8. Experimental test bench [26].

In Step #1, a 0.5-Hz sinusoidal current with an amplitude of 0.5 C was injected, as shown in Fig. 9(a). The first-order Butterworth high-pass filter used had a 3-dB bandwidth of 0.05 Hz. As shown in Fig. 9(b), the estimated R_s can accurately track the actual value. In Step #2, a 0.02-Hz sinusoidal current with an amplitude of 0.5 C was added to a "base" current (0.004 Hz sinusoidal current with amplitude of 0.5 C), as shown in Fig. 9(a).

The first-order Butterworth high-pass filter used had a 3-dB bandwidth of 0.002 Hz. By using the estimated R_s, the estimated

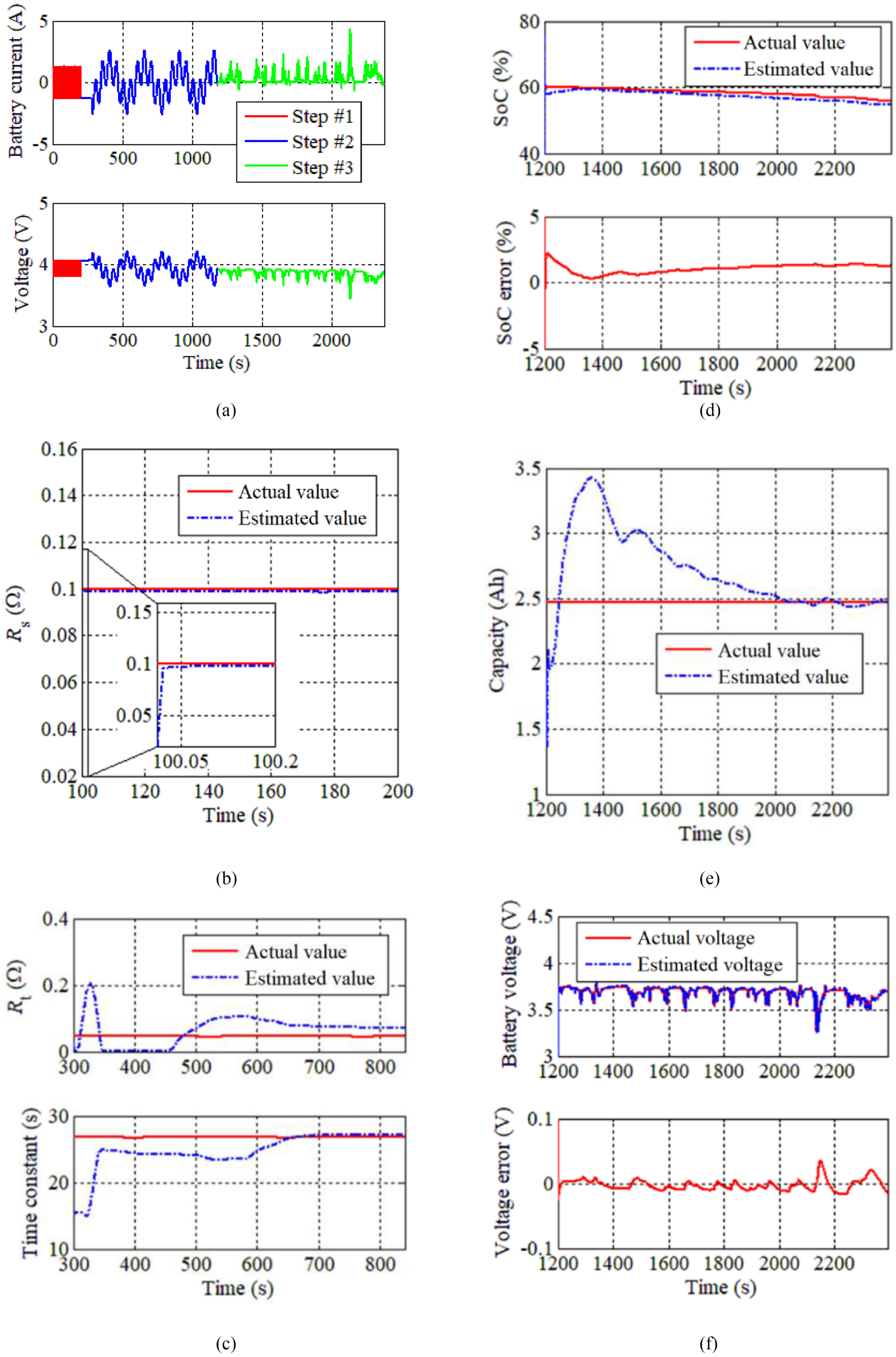

Fig. 9. Experimental results. (a) Battery current profile. (b) R_s estimation result (Step #1). (c) R_t and τ estimation result (Step #2). (d) SoC estimation result (Step #3). (e) Q_b estimation result (Step #3). (f) v_b estimation result (Step #3).

R_t and τ can largely track the real values, even though the estimated R_t has a static error when compared to its "actual value," as shown in Fig. 9(c). This indicates that the first-order ECM model has limitations, since the *RC* pair is difficult to be characterized and estimated.

Finally, in Step #3, the estimated R_s, R_t, and τ are used to estimate SoC and SoH concurrently. A scaled bus driving cycle is used in Step #3 to represent a practical current profile for the battery. As shown in Fig. 9(d), the SoC estimation is accurate given that the estimated error is below 1.5% under a significant initial error (30%). As shown in Fig. 9(e), the estimated capacity Q_b converges to the actual value, which is obtained from the static capacity test, and there is no obvious error after convergence. Since all parameters/states are well estimated, the estimated terminal voltage also tracks the actual value well, as shown in Fig. 9(f).

Experimental results for the multiparameter case have been shown in [17] and [18] using the same Samsung 18650 battery cell. Due to space limitations, the experimental comparison is not provided in this article. Based on the experimental results provided in [17] and [18], it is clear that the sequential algorithm achieves much better estimation performance when compared to the multiparameter case.

In terms of the implementation of the proposed method, we point out that if the battery is the only power source, it is difficult to inject the high-frequency current while keeping the system operating normally since the battery needs to satisfy the power demand. It may be feasible to manipulate the battery charging profile to inject the desired current signals for the parameter/state estimation; however, it is still difficult to implement the proposed algorithm as the charging process is not easy to be changed in most battery-only applications (e.g., the charging station for electric vehicles). Especially, when the battery parameters under charging conditions significantly differ from the ones under discharging conditions, it is difficult to use the proposed sequential algorithm as the parameters, which are estimated in charging processes, cannot be used in discharging processes.

Furthermore, when the battery is adopted in overactuated systems (e.g., the battery/supercapacitor hybrid energy storage system and hybrid electric vehicles), which have the additional power source and only follow one power demand, the desired current signals and output regulation objectives can be achieved concurrently, and estimation over a long period may not interrupt the normal operation. The optimal current for parameter identification of battery can be compensated by the other power source (e.g., supercapacitor). In addition, since the sinusoidal current is injected in the battery current profile, the corresponding compensation current for the other power source would not continuously drain its energy, meaning that it can be produced indefinitely. Specifically, given that the battery voltage is generally stable, the sinusoidal signal injected in battery will induce a corresponding sinusoidal power demand to the supercapacitor, meaning that the supercapacitor is not required to constantly discharge (or charge). For example, when there is no power demand from the load, the supercapacitor only needs to provide a periodic current with an average value of zero to compensate the injected signal. Therefore, only a small amount of energy is consumed due to losses in the power electronic components. In addition, without disturbing the current injection, the battery can be used to charge the supercapacitor in practical applications.

We note that the estimation process of the *RC* parameters takes a long time since R_t does not entirely converge to its actual value at 800 s, as shown in Fig. 9(c), and this may pose some problems in practical applications. We would like to point out that the *RC* voltage is small for the studied battery cell, therefore, the estimation of *RC* parameters is inherently difficult, but this in turn gives us some hints that the *RC* parameters can be potentially neglected for this specific battery cell when focusing on the SoC/SoH estimation from the battery modeling perspective, since the *RC* voltage only slightly contributes to the battery terminal voltage and, hence, would not significantly influence the SoC/SoH estimation accuracy. In future work, the tradeoff between the model complexity and the estimation accuracy of battery states (e.g., SoC and SoH) will be further investigated.

VI. Conclusion

The estimation of battery parameters and states based on a first-order ECM is studied in this article. The CR bound is used to evaluate the parameter/state estimation accuracy for three cases: the single-parameter case, the multiparameter case, and the sequential algorithm case. The analysis shows the possibility of improving estimation accuracy by injecting PE signals into the current waveform and estimating the parameters/states sequentially. The CR bound analysis shows that the estimation accuracy of sequential estimation is much better than that of the multiparameter case. The effectiveness of sequential estimation is verified by simulation results. The initial experimental result is also provided to further validate the proposed algorithm.

We note that the proposed algorithm is designed for overactuated systems, since the overactuation feature can be exploited for the active current injection. For the battery-only applications (e.g., electric vehicles), the feasibility of the proposed method should be further evaluated and it has limitations because generally, the battery current profile cannot be changed for the signal injection.

Acknowledgment

The authors would like to thank Dr. X. Wu and Mr. X. Li from the Harbin University of Science and Technology, Harbin, China, for their help with the experiments.

References

[1] L. Lu, X. Han, J. Li, J. Hua, and M. Ouyang, "A review on the key issues for lithium-ion battery management in electric vehicles," *J. Power Sources*, vol. 226, pp. 272–288, Mar. 2013.

[2] J. Zhang and J. Lee, "A review on prognostics and health monitoring of Li-ion battery," *J. Power Sources*, vol. 196, pp. 6007–6014, Aug. 2011.

[3] R. Xiong, F. Sun, Z. Chen, and H. He, "A data-driven multi-scale extended Kalman filtering based parameter and state estimation approach of lithium-ion polymer battery in electric vehicles," *Appl. Energy*, vol. 113, pp. 463–476, Jan. 2014.

[4] X. Hu, S. E. Li, and H. Peng, "A comparative study of equivalent circuit models for Li-ion batteries," *J. Power Sources*, vol. 198, pp. 359–367, Jan. 2012.

[5] M. Charkhgard and M. Farrokhi, "State-of-charge estimation for lithium-ion batteries using neural networks and EKF," *IEEE Trans. Ind. Electron.*, vol. 57, no. 12, pp. 4178–4187, Dec. 2010.

[6] X. Lin and A. Stefanopoulou, "Analytic bound on accuracy of battery state and parameter estimation," *J. Electrochem. Soc.*, vol. 162, no. 9, pp. A1879–A1891, 2015.

[7] P. Ioannou and J. Sun, *Robust Adaptive Control*, vol. 1. North Chelmsford, MA, USA: Courier Corporation, 2012.

[8] X. Lin, "A data selection strategy for real-time estimation of battery parameters," in *Proc. Amer. Control Conf.*, 2018, pp. 2276–2281.

[9] Z. Song, J. Hou, H. Hofmann, X. Lin, and J. Sun, "Parameter identification and maximum power estimation of battery/supercapacitor hybrid energy storage system based on Cramer–Rao bound analysis," *IEEE Trans. Power Electron.*, vol. 34, no. 5, pp. 4831–4843, May 2019.

[10] P. Mishra, M. Garg, S. Mendoza, J. Liu, C. Rahn, and H. Fathy, "How does model reduction affect lithium-ion battery state of charge estimation errors? Theory and experiments," *J. Electrochem. Soc.*, vol. 164, no. 2, pp. A237–A251, 2017.

[11] X. Lin, "Analytic analysis of the data-dependent estimation accuracy of battery equivalent circuit dynamics," *IEEE Control Syst. Lett.*, vol. 1, no. 2, pp. 304–309, Jun. 2017.

[12] A. Klintberg, T. Wik, and B. Fridholm, "Theoretical bounds on the accuracy of state and parameter estimation for batteries," in *Proc. Amer. Control Conf.*, 2017, pp. 4035–4041.

[13] M. Rothenberger, D. Docimo, M. Ghanaatpishe, and H. Fathy, "Genetic optimization and experimental validation of a test cycle that maximizes parameter identifiability for a Li-ion equivalent-circuit battery model," *J. Energy Storage*, vol. 4, pp. 156–166, Dec. 2015.

[14] M. Rothenberger, J. Anstrom, S. Brennan, and H. Fathy, "Maximizing parameter identifiability of an equivalent-circuit battery model using optimal periodic input shaping," in *Proc. ASME Dyn. Syst. Control Conf.*, 2014, Art. no. V001T19A004.

[15] X. Lin, "Theoretical analysis of battery SOC estimation errors under sensor bias and variance," *IEEE Trans. Ind. Electron.*, vol. 65, no. 9, pp. 7138–7148, Sep. 2018.

[16] Y. Zheng, M. Ouyang, X. Han, L. Lu, and J. Li, "Investigating the error sources of the online state of charge estimation methods for lithium-ion batteries in electric vehicles," *J. Power Sources*, vol. 377, pp. 161–188, Feb. 2018.

[17] Z. Song, X. Wu, X. Li, J. Sun, H. Hofmann, and H. Jun, "Current profile optimization for combined state of charge and state of health estimation of Lithium ion battery based on Cramer–Rao bound analysis," *IEEE Trans. Power Electron.*, vol. 34, no. 7, pp. 7067–7078, Jul. 2018.

[18] Z. Song *et al.*, "The sequential algorithm for combined state of charge and state of health estimation of lithium ion battery based on active current injection," 2019, *arXiv preprint arXiv:1901.06000v2*.

[19] J. Xu, C. Mi, B. Cao, and J. Cao, "A new method to estimate the state of charge of lithium-ion batteries based on the battery impedance model," *J. Power Sources*, vol. 233, pp. 277–284, Jul. 2013.

[20] D. Di Domenico, A. Stefanopoulou, and G. Fiengo, "Lithium-ion battery state of charge and critical surface charge estimation using an electrochemical model-based extended Kalman filter," *J. Dyn. Syst. Meas. Control*, vol. 132, no. 6, Oct. 2010, Art. no. 061302.

[21] C. Weng, Y. Cui, J. Sun, and H. Peng, "On-board state of health monitoring of lithium-ion batteries using incremental capacity analysis with support vector regression," *J. Power Sources*, vol. 235, pp. 36–44, Aug. 2013.

[22] J. Wei, G. Dong, and Z. Chen, "Remaining useful life prediction and state of health diagnosis for lithium-ion batteries using particle filter and support vector regression," *IEEE Trans. Ind. Electron.*, vol. 65, no. 7, pp. 5634–5643, Jul. 2018.

[23] X. Lin *et al.*, "A lumped-parameter electro-thermal model for cylindrical batteries," *J. Power Sources*, vol. 257, pp. 1–11, Jul. 2014.

[24] N. Samad, J. Siegel, and A. Stefanopoulou, "Parameterization and validation of a distributed coupled electro-thermal model for prismatic cells," in *Proc. ASME Dyn. Syst. Control Conf.*, 2014, Art. no. V002T23A006.

[25] H. He, R. Xiong, X. Zhang, F. Sun, and J. Fan, "State-of-charge estimation of the lithium-ion battery using an adaptive extended Kalman filter based on an improved Thevenin model," *IEEE Trans. Veh. Technol.*, vol. 60, no. 4, pp. 1461–1469, Mar. 2011.

[26] X. Wu, X. Li, and J. Du, "State of charge estimation of lithium-ion batteries over wide temperature range using unscented Kalman filter," *IEEE Access*, vol. 6, pp. 41993–42003, Aug. 2018.

Ziyou Song (M'18) received the B.E. (with honor) and Ph.D. (with highest honor and thesis award) degrees in automotive engineering from Tsinghua University, Beijing, China, in 2011 and 2016, respectively.

He was a Research Scientist with Tsinghua University from 2016 to 2017 and is currently a Postdoctoral Research Fellow with the Department of Naval Architecture and Marine Engineering and Department of Electrical Engineering and Computer Science, University of Michigan, Ann Arbor, MI, USA. He is the author or co-author of more than 50 peer-reviewed publications including 40 journal articles. His research interests include modeling, estimation, optimization, and control of energy storage for electrified vehicles and renewable systems.

Dr. Song was the recipient of several paper awards, including Applied Energy Highly Cited Paper Award 2015–2016, Applied Energy Award for Most Cited Energy Article from China, NSK Outstanding Paper Award of Mechanical Engineering, and 2013 IEEE VPPC Best Student Paper Award.

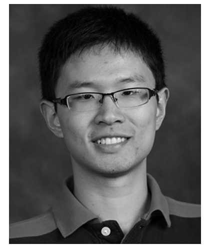

Hao Wang received the B.E. degree in vehicle engineering from the Hefei University of Technology, Hefei, China, in 2012, and the M.S.E. degree in mechanical engineering in 2014 from the University of Michigan, Ann Arbor, MI, USA, where he is currently working toward the Ph.D. degree in naval architecture and marine engineering.

His current research interests include set-membership identification and its applications, energy management of integrated power and thermal management systems, and applications to electrified vehicles.

Jun Hou (S'15–M'18) received the M.S. degree in electrical engineering from Northeastern University, Shenyang, China, in 2011, and the Ph.D. degree from the University of Michigan, Ann Arbor, MI, USA, in 2017.

His current research interests include integration, modeling, control, and optimization of hybrid energy storage, power electronic converters, and electric propulsion systems.

Heath F. Hofmann (S'90–M'92–SM'16) received the Ph.D. degree in electrical engineering and computer science from the University of California at Berkeley, Berkeley, CA, USA, in 1998.

He is currently a Professor with the University of Michigan, Ann Arbor, MI, USA. He has authored approximately four dozen papers in refereed journals. He currently holds 14 patents. His research interests include power electronics, specializing in the design, simulation, and control of electromechanical systems, adaptive control techniques, energy harvesting, flywheel energy storage systems, electric and hybrid electric vehicles, and finite-element analysis.

Jing Sun (M'89–SM'00–F'04) received the B.S. and M.S. degrees from the University of Science and Technology of China, Hefei, China, in 1982 and 1984, respectively, and the Ph.D. degree from the University of Southern California, Los Angeles, CA, USA, in 1989.

From 1989–1993, she was an Assistant Professor with the Department of Electrical and Computer Engineering, Wayne State University. She joined the Ford Research Laboratory in 1993, where she was with the Department of Powertrain Control Systems. After spending almost ten years in industry, she came back to academia and joined the faculty of the College of Engineering, University of Michigan, Ann Arbor, MI, USA, in 2003, where she is currently the Michael G. Parsons Professor and the Chair with the Department of Naval Architecture and Marine Engineering, with courtesy appointments as a Professor with the Department of Electrical Engineering and Computer Science and Department of Mechanical Engineering. She holds 39 US patents and has coauthored a textbook on robust adaptive control. Her research interests include system and control theory and its applications to marine and automotive propulsion systems.

Prof. Sun was a recipient of the 2003 IEEE Control System Technology Award.